



Targeting CXCR4-dependent immunosuppressive Ly6C^{low} monocytes improves antiangiogenic therapy in colorectal cancer

Keehoon Jung^{a,1}, Takahiro Heishi^{a,1}, Joao Incio^a, Yuhui Huang^a, Elizabeth Y. Beech^a, Matthias Pinter^a, William W. Ho^{a,b}, Kosuke Kawaguchi^a, Nuh N. Rahbari^a, Euiheon Chung^{a,2}, Jun Ki Kim^{c,3}, Jeffrey W. Clark^d, Christopher G. Willett^e, Seok Hyun Yun^{c,f}, Andrew D. Luster^g, Timothy P. Padera^a, Rakesh K. Jain^{a,4,5}, and Dai Fukumura^{a,4,5}

^aEdwin L. Steele Laboratories for Tumor Biology, Department of Radiation Oncology, Harvard Medical School and Massachusetts General Hospital, Boston, MA 02114; ^bDepartment of Chemical Engineering, Massachusetts Institute of Technology, Cambridge, MA 02139; ^cWellman Center for Photomedicine, Department of Dermatology, Harvard Medical School and Massachusetts General Hospital, Boston, MA 02114; ^dDepartment of Hematology/Oncology, Harvard Medical School and Massachusetts General Hospital, Boston, MA 02114; ^eDepartment of Radiation Oncology, Duke University Medical Center, Durham, NC 27710; ^fDivision of Health Sciences and Technology, Harvard–Massachusetts Institute of Technology, Cambridge, MA 02139; and ^gCenter for Immunology and Inflammatory Diseases, Division of Rheumatology, Allergy and Immunology, Harvard Medical School and Massachusetts General Hospital, Boston, MA 02114

Contributed by Rakesh K. Jain, August 10, 2017 (sent for review June 19, 2017; reviewed by Timothy T. Hla and Judith A. Varner)

Antiangiogenic therapy with antibodies against VEGF (bevacizumab) or VEGFR2 (ramucirumab) has been proven efficacious in colorectal cancer (CRC) patients. However, the improvement in overall survival is modest and only in combination with chemotherapy. Thus, there is an urgent need to identify potential underlying mechanisms of resistance specific to antiangiogenic therapy and develop strategies to overcome them. Here we found that anti-VEGFR2 therapy up-regulates both C-X-C chemokine ligand 12 (CXCL12) and C-X-C chemokine receptor 4 (CXCR4) in orthotopic murine CRC models, including SL4 and CT26. Blockade of CXCR4 signaling significantly enhanced treatment efficacy of anti-VEGFR2 treatment in both CRC models. CXCR4 was predominantly expressed in immunosuppressive innate immune cells, which are recruited to CRCs upon anti-VEGFR2 treatment. Blockade of CXCR4 abrogated the recruitment of these innate immune cells. Importantly, these myeloid cells were mostly Ly6C^{low} monocytes and not Ly6C^{high} monocytes. To selectively deplete individual innate immune cell populations, we targeted key pathways in Ly6C^{low} monocytes (Cx3cr1^{-/-} mice), Ly6C^{high} monocytes (CCR2^{-/-} mice), and neutrophils (anti-Ly6G antibody) in combination with CXCR4 blockade in SL4 CRCs. Depletion of Ly6C^{low} monocytes or neutrophils improved anti-VEGFR2-induced SL4 tumor growth delay similar to the CXCR4 blockade. In CT26 CRCs, highly resistant to anti-VEGFR2 therapy, CXCR4 blockade enhanced anti-VEGFR2-induced tumor growth delay but specific depletion of Ly6G⁺ neutrophils did not. The discovery of CXCR4-dependent recruitment of Ly6C^{low} monocytes in tumors unveiled a heretofore unknown mechanism of resistance to anti-VEGF therapies. Our findings also provide a rapidly translatable strategy to enhance the outcome of anti-VEGF cancer therapies.

tumor microenvironment | CXCR4 | Ly6C^{low} monocyte | tumor immunity | antiangiogenic therapy

Antivascular endothelial growth factor (anti-VEGF) therapy is widely used in many types of solid tumors and is the current standard of care for metastatic colorectal cancer (CRC) (1). However, the beneficial effects from anti-VEGF therapy are often short-lived due to intrinsic resistance and/or resistance acquired during the treatment (1–8). Therefore, it is critical to identify mechanisms and/or biomarkers of resistance to target these mechanisms and/or to stratify patients by biomarkers to improve the clinical outcome. We recently found that Ly6C^{low} monocytes infiltrate into tumors in a C-X3-C chemokine receptor 1 (CX3CR1)-dependent manner and confer resistance to anti-VEGFR2 therapy (9). However, there is no clinically available agent targeting this pathway, which significantly limits the possibility of clinical translation.

We previously reported up-regulation of C-X-C chemokine receptor 4 (CXCR4) and its ligand C-X-C chemokine ligand 12

(CXCL12)—also known as stromal cell-derived factor-1 alpha (SDF-1 α)—in primary tumor biopsies from rectal cancer patients treated with the anti-VEGF antibody bevacizumab compared with baseline in the same patients (10, 11). However, the role of CXCL12/CXCR4 signaling in the resistance to anti-VEGF CRC therapy is not fully understood. While the role of CXCL12/CXCR4

Significance

The survival benefit of antiangiogenic therapies for cancer patients has been limited, potentially due to intrinsic/acquired resistance. Deciphering and targeting resistance mechanisms are critical to improving treatment outcome, especially in cancers where antiangiogenic therapies are standard of care, such as colorectal cancer (CRC). Consistent with our clinical findings, we found up-regulation of CXCL12/CXCR4 in orthotopic CRC models and conditional *Apc* mutant spontaneous rectal tumors after anti-VEGFR2 treatment. CXCR4 signaling recruited immunosuppressive innate immune cells such as Ly6C^{low} monocytes and Ly6G⁺ neutrophils to the CRCs, conferring resistance to VEGFR2 blockade. Furthermore, we successfully targeted these pathways genetically and pharmacologically, including with an FDA-approved agent Plerixafor (AMD3100), which significantly enhanced treatment response. These strategies have the potential for rapid clinical translation.

Author contributions: K.J., A.D.L., T.P.P., R.K.J., and D.F. designed research; K.J., T.H., J.I., Y.H., E.Y.B., M.P., W.W.H., K.K., N.N.R., E.C., and J.K.K. performed research; J.W.C. and C.G.W. contributed new reagents/analytic tools; K.J., T.H., S.H.Y., A.D.L., T.P.P., R.K.J., and D.F. analyzed data; and K.J., S.H.Y., T.P.P., R.K.J., and D.F. wrote the paper.

Reviewers: T.T.H., Boston Children's Hospital and Harvard Medical School; and J.A.V., University of California, San Diego.

Conflict of interest statement: R.K.J. received consultant fees from Merck, Ophthotech, Pfizer, SPARC, SynDevRx, and XTuit; owns equity in Enlight, Ophthotech, SynDevRx, and XTuit; and serves on the Board of Directors of XTuit and the Boards of Trustees of Tekla Healthcare Investors, Tekla Life Sciences Investors, Tekla Healthcare Opportunities Fund, and Tekla World Healthcare Fund. Neither any reagent nor any funding from these organizations was used in this study.

Freely available online through the PNAS open access option.

¹K.J. and T.H. contributed equally to this work.

²Present address: Department of Medical System Engineering, School of Mechatronics, Gwangju Institute of Science and Technology, Gwangju 500-712, Republic of Korea.

³Present address: Biomedical Engineering Research Center, Asan Institute for Life Sciences, Asan Medical Center, University of Ulsan College of Medicine, Seoul 05505, Republic of Korea.

⁴R.K.J., and D.F. contributed equally to this work.

⁵To whom correspondence may be addressed. Email: jain@steele.mgh.harvard.edu or dai@steele.mgh.harvard.edu.

This article contains supporting information online at www.pnas.org/lookup/suppl/doi:10.1073/pnas.1710754114/-DCSupplemental.

axis in regulation of immune cells has been investigated, including a subset of monocytes (i.e., Ly6C^{high} monocytes) (12–17), whether CXCR4 is involved in regulation of another subset of monocytes (i.e., Ly6C^{low} monocytes) is not known.

In this study, building on our previous clinical finding that CXCR4 is up-regulated in rectal cancer postbevacizumab therapy, we targeted CXCR4 using AMD3100, an FDA approved agent, which resulted in significant improvement of anti-VEGFR2 therapy in clinically relevant orthotopic murine CRC models. Mechanistically, we found that CXCR4 is critical for tumor infiltration of Ly6C^{low} monocytes and that blockade of Ly6C^{low} monocyte recruitment improves the efficacy of anti-VEGFR2 therapy in CRCs. Thus, targeting CXCR4-mediated Ly6C^{low} monocyte infiltration is a potential strategy to enhance the efficacy of anti-VEGF treatments for CRC patients.

Results

Antiangiogenic Therapy Increases Expression of CXCL12 and CXCR4 in CRCs. We treated two different orthotopic colon cancer models—SL4 and CT26—as well as a spontaneous rectal tumor model in *Apc* conditional knockout mice with a monoclonal antibody (DC101) targeting VEGF receptor 2 (VEGFR2) (18). We have previously demonstrated that CXCL12 and CXCR4 expression increases in primary human rectal tumors of patients treated with bevacizumab monotherapy (10, 11). Consistent with these clinical data (11), we found a significant increase in CXCR4 and CXCL12 expression after DC101 treatment in both spontaneous rectal tumors and established CRCs (Fig. 1 *A–D* and Fig. S1). These findings indicate that our CRC models recapitulate the response of primary human CRCs to bevacizumab.

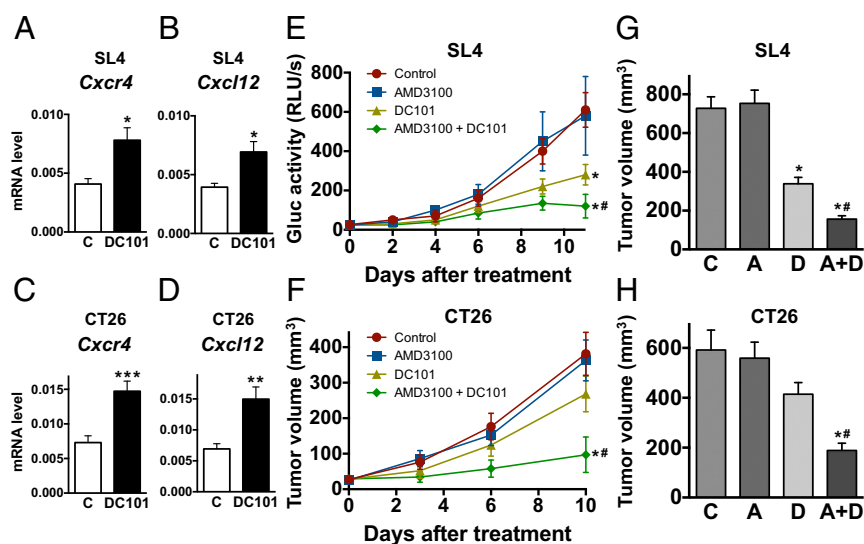
Blockade of CXCR4 Enhances the Antitumor Effect of Anti-VEGFR2 Therapy. We next examined the role of CXCL12/CXCR4 signaling in the resistance to anti-VEGFR2 therapy in CRCs using an FDA-approved CXCR4 inhibitor (AMD3100) (19). In both SL4 and CT26 models, we found that treating with AMD3100 significantly enhanced the antitumor effect of anti-VEGFR2 (DC101) therapy, resulting in delayed tumor growth and increased survival of animals (Fig. 1 *E–H* and Figs. S2–S4). Interestingly, SL4 tumors were more sensitive to DC101 therapy than CT26 tumors, representing the heterogeneity in patient response. As

we have previously shown (9), SL4 and CT26 tumor size was ~45% and ~70% of that of the control after 12 d of DC101 monotherapy (Fig. 1 *G* and *H*). In addition, the extent of tumor growth inhibition by the combined therapy was similar in both SL4 and CT26 models. These data indicate that the mechanism making CT26 less sensitive to anti-VEGFR2 treatment was abolished by the blockade of CXCR4. These data show that targeting CXCR4 enhances the efficacy of antiangiogenic therapy in both CRC models, regardless of their sensitivity to anti-VEGFR2 monotherapy.

Blockade of CXCR4 Alleviates Anti-VEGFR2 Therapy-Induced Lymphocyte Reduction but Does Not Directly Affect Tumor Cell Proliferation. Next, we sought the mechanisms of how the blockade of CXCR4 enhances the antitumor effect of anti-VEGFR2 therapy. First, we tested whether the blockade of CXCR4 directly inhibited proliferation of cancer cells themselves. MTT (methyl thiazolyl tetrazolium) assay results showed that CXCR4 is not involved in the regulation of colon cancer cell proliferation (Fig. S5). Given the important role of CXCR4 in chemotaxis of leukocytes (20, 21), we next examined the effect of AMD3100 and DC101 on the immune microenvironment. We analyzed lymphoid populations in SL4 and CT26 tumors and found fewer CD4⁺ (SL4, 3.7 ± 0.8% in control vs. 1.7 ± 0.3% in DC101 and CT26, 4.4 ± 0.9% in control vs. 2.5 ± 0.4% in DC101) and CD8⁺ T cells (SL4, 4.1 ± 0.8% in control vs. 2.3 ± 0.7% in DC101 and CT26, 8.9 ± 1.7% in control vs. 4.1 ± 1.2% in DC101) in the DC101-treated group (Fig. S6). We also found that AMD3100 treatment restored the number of T lymphocytes to the level of control rat IgG-treated tumors (Fig. S6). Given that effector CD4⁺ and CD8⁺ T cells are known to express CXCR4 in some contexts (22, 23), we measured the expression of CXCR4 on these lymphocytes. However, to our surprise, we observed only a negligible level of CXCR4 expression on T lymphocytes in the CRC microenvironment (Fig. S7). Based on these findings, we explored whether the effect of AMD3100 treatment on the inhibition of T-cell infiltration is indirect and mediated by other immune cell types expressing CXCR4.

CXCR4 Is Predominantly Expressed by Monocytes and Neutrophils in the Immune Microenvironment in CRCs. While we found that CD4⁺/CD8⁺ T lymphocytes and natural killer cells do not appreciably express CXCR4, we found abundant expression of CXCR4 in myeloid cell

Fig. 1. Anti-VEGFR2 therapy increases expression of CXCL12/CXCR4 in CRCs and blockade of CXCR4 enhances the antitumor effect of anti-VEGFR2 therapy. (*A* and *B*) Gene expression levels for *Cxcr4* (*A*) and *Cxcl12* (*B*) in SL4 tumor. C57BL/6 WT mice bearing orthotopically grown syngeneic SL4-Gluc CRCs were treated with either control rat IgG (*C*) or monoclonal anti-VEGFR2 antibody, DC101 (40 mg/kg, every 3 d). One week after treatment, CXCR4 and CXCL12 mRNA expression levels in CRCs were determined by quantitative real-time PCR, normalized against GAPDH. Data are presented as mean ± SEM *n* = 5 per group. **P* < 0.05 vs. control. (*C* and *D*) Gene expression levels for *Cxcr4* (*C*) and *Cxcl12* (*D*) in CT26 tumor. CT26 tumors in BALB/c wild-type mice were treated with either IgG control (*C*) or monoclonal anti-VEGFR2 antibody, DC101 (40 mg/kg, every 3 d). One week after treatment, relative CXCR4 and CXCL12 mRNA expression levels in CRCs were determined by quantitative real-time PCR, normalized against GAPDH. *n* = 5 per group. **P* < 0.05 vs. control. ***P* < 0.04 vs. control. ****P* < 0.03 vs. control. (*E*) SL4 tumor burden was assessed by blood Gluc activity measurement (53). Data are represented as mean ± SEM *n* = 8 per group. (*F*) CT26 tumor volume was measured using a high-frequency ultrasound imaging system (3). Data are represented as mean ± SEM *n* = 8 per group. **P* < 0.05 vs. corresponding control. #*P* < 0.05 vs. corresponding DC101 treatment group. (*G* and *H*) Tumor volume of SL4 (*G*) and CT26 (*H*) measured on day 12 after treatment (A, AMD3100; A+D; AMD3100 + DC101; C, control; D, DC101). Data are represented as mean ± SEM, *n* = 8 per group. **P* < 0.05 vs. corresponding control. #*P* < 0.05 vs. corresponding DC101 group.



populations in CRC tissues upon DC101 treatment (Fig. S7). Consistent with these findings and our previous studies in other types of tumors (24), we observed an increase in CD11b⁺Gr1⁺ cells in DC101-treated tumors shown by flow cytometry (Fig. S8). In fact, the CD11b⁺Gr1⁺ cells represent a heterogeneous mixture of myeloid cells that include monocytes and neutrophils. Thus, we subdivided the CD11b⁺Gr1⁺ myeloid cells and analyzed these subpopulations separately (i.e., Ly6C^{high} monocytes and Ly6G⁺ neutrophils) based on their immunophenotype using appropriate surface markers. These CD11b⁺Gr1⁺ cells were previously implicated in resistance to anti-VEGF therapy (2, 25). We also found abundant expression of CXCR4 in another monocyte subset—Ly6C^{low} monocytes—which do not belong to the CD11b⁺Gr1⁺ myeloid cells (Fig. S7). Of note, these myeloid cells are devoid of F4/80 and CD11c expression. Hence, they do not appear to be tumor associated macrophages (TAMs) or dendritic cells (DCs) (Fig. S9).

Blockade of CXCR4 Inhibits Anti-VEGFR2 Therapy-Induced Tumor Infiltration of Ly6C^{low} Monocytes and Ly6G⁺ Neutrophils. We have previously analyzed these three different myeloid cell subpopulations expressing CXCR4 (i.e., Ly6C^{low} monocytes, Ly6C^{high} monocytes, and Ly6G⁺ neutrophils) during the course of anti-VEGFR2 therapy (9). Consistent with our prior work, we found DC101 treatment significantly increased the number of Ly6C^{low} monocytes on day 5 and day 12 (Fig. 2) in SL4 and CT26 tumors. Also, there was a significant increase in the number of neutrophils on day 12 after DC101 treatment in both tumor models (Fig. 2B and D). The number of Ly6C^{high} monocytes was much lower than the other two subpopulations and did not change upon anti-VEGFR2 therapy (Fig. 2). In addition, the fractions of Ly6C^{low} monocytes and Ly6G⁺ neutrophils to CD45⁺ cells were higher in CT26 than in SL4 tumors after DC101 treatment, which seems consistent with the differences in growth behavior of CT26 (“DC101 resistant” as shown in Fig. 1F and H) and SL4 tumors (“DC101 sensitive”) (Fig. 1E and G).

In both SL4 and CT26 tumors, consistent with our previous findings (9), we observed that Ly6C^{low} monocytes infiltrate into tumors before neutrophils (Fig. 2). Furthermore, AMD3100 treatment inhibited DC101-induced Ly6C^{low} monocyte and neutrophil accumulation (Fig. 2B and D), which is consistent with our hypothesis and leads to the improved antitumor efficacy that we observed (Fig. 1E and F).

In Anti-VEGFR2-Sensitive SL4 Tumors, Blockade of CXCR4-Dependent Infiltration of Ly6C^{low} Monocytes or Ly6G⁺ Neutrophils Improves Efficacy of Anti-VEGFR2 Therapy. Next, we performed a series of experiments depleting individual subsets of myeloid cells. Ly6C^{low} monocytes express a high level of CX3CR1, and their infiltration is dependent on this chemokine receptor (26–28). We specifically inhibited the infiltration of Ly6C^{low} monocytes by using *Cx3cr1*^{-/-} mice as described previously (9, 29, 30). Using *Cx3cr1*^{-/-} mice, we also confirmed our earlier observation of impaired recruitment of Ly6G⁺ neutrophils, which arrive after Ly6C^{low} monocytes (9) (Fig. S10). DC101 monotherapy in wild-type mice exhibited modest tumor growth delay and survival benefit (Fig. 3A and Fig. S4A). AMD3100 treatment in combination with DC101 in wild-type mice showed a further improvement in antitumor efficacy (Fig. 3A and Fig. S4A). The antitumor efficacy of combinatorial treatment of AMD3100 and DC101 in wild-type mice was comparable to that of DC101 monotherapy in *Cx3cr1*^{-/-} mice (Fig. 3A). However, there was no further improvement in antitumor efficacy by AMD3100 treatment in *Cx3cr1*^{-/-} mice (Fig. 3A). Using *Ccr2*^{-/-} mice to specifically inhibit infiltration of Ly6C^{high} monocytes, there was no difference in antitumor efficacy from any of the tested treatments between wild-type and *Ccr2*^{-/-} mice (Fig. 3B). Lastly, using an anti-Ly6G neutralizing antibody to deplete neutrophils, antitumor efficacy was improved when combined with DC101 (Fig. 3C), similar to the effect of combined AMD3100 and DC101.

In Anti-VEGFR2-Resistant CT26 Tumors, Blockade of both Ly6C^{low} Monocyte and Ly6G⁺ Neutrophil Infiltration Is Needed to Improve the Efficacy of Anti-VEGFR2 Therapy. As shown, CT26 tumors are more refractory to anti-VEGFR2 (Fig. 1E and F) and have a higher number of Ly6C^{low} monocytes than SL4 tumors (Fig. 2). Thus, we asked whether the inhibition of neutrophil infiltration in CT26 tumors is sufficient to improve the efficacy of anti-VEGFR2 therapy as observed in SL4 tumors (Fig. 3C). We used anti-Ly6G antibody to specifically deplete neutrophils in the CT26 model. Interestingly, even with the successful depletion of neutrophils after anti-Ly6G antibody treatment, we did not observe any significant improvement in antitumor efficacy from the combination treatment of DC101 and anti-Ly6G antibody compared with DC101 monotherapy (Fig. 4). Meanwhile, when we treated AMD3100 along with DC101, there was a dramatic enhancement in antitumor efficacy compared with DC101 monotherapy in CT26 tumors (Fig. 4 and Fig. S4B). Thus, we

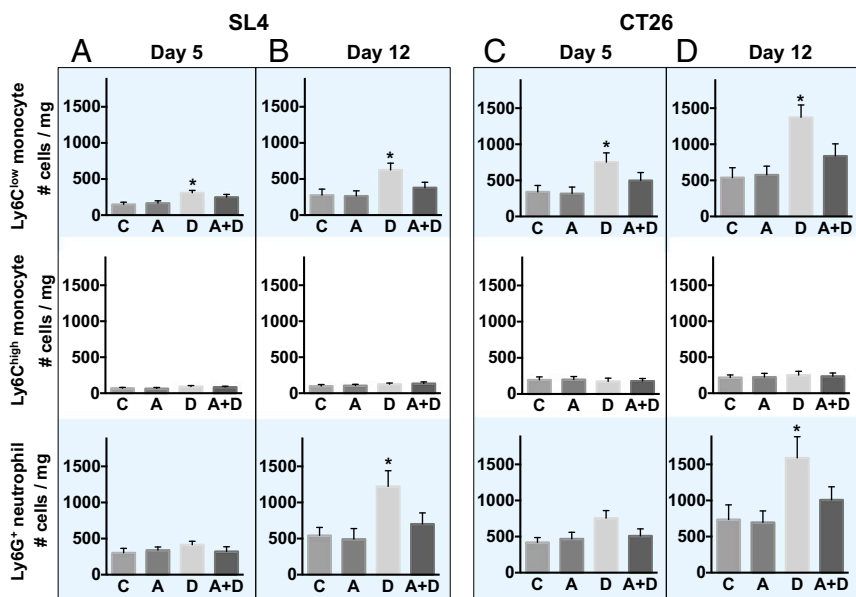


Fig. 2. Blockade of CXCR4 inhibits anti-VEGFR2 therapy-induced infiltration of Ly6C^{low} monocytes and Ly6G⁺ neutrophils. (A and B) Three subpopulations of myeloid cells (Ly6C^{low} and Ly6C^{high} monocytes) and Ly6G⁺ neutrophils in SL4 tumors. C57BL/6 WT mice bearing SL4 CRCs were treated with either control IgG (C), AMD3100 (A), DC101 (D), or AMD3100 + DC101 (A+D). Each myeloid cell subset in tumors was analyzed by flow cytometry on days 5 (A) and 12 (B). (Top row) Ly6C^{low} monocyte. (Center row) Ly6C^{high} monocyte. (Bottom row) Ly6G⁺ neutrophil. Data are represented as mean ± SEM, *n* = 7 per group. **P* < 0.05 vs. control. The graphs depict the absolute number of cells per milligram of tumor tissue. (C and D) Three subpopulations of myeloid cells in CT26 tumors. CT26 tumors in wild-type mice were divided into four different treatment groups (C, A, D, A+D), and each subset of myeloid cells in the tumor infiltrate were analyzed on days 5 (C) and 12 (D) by flow cytometry. Data are represented as mean ± SEM, *n* = 7 per group. **P* < 0.05 vs. control. The graphs depict the absolute number of cells per milligram of tumor tissue.

conclude that blockade of CXCR4—which efficiently inhibits infiltration of both Ly6C^{low} monocytes and neutrophils—is more effective than targeting neutrophils alone. Therefore, it is critical to target Ly6C^{low} monocytes to improve anti-VEGFR2 therapy efficacy especially in CRCs highly refractory to the treatment.

Discussion

In this study, we first verified that the findings from our preclinical CRC models recapitulate the key findings of our previous clinical studies on CRC patients with anti-VEGF therapy—namely up-regulation of CXCL12/CXCR4 pathway after a single dose of bevacizumab (31). Our preclinical models allowed a causal study of this signaling pathway using a clinically available CXCR4 inhibitor (AMD3100). Furthermore, we found that targeting Ly6C^{low} monocytes is essential to improve antitumor efficacy of anti-VEGFR2 therapy in tumors highly resistant to the therapy, such as CT26. The elevated numbers of Ly6C^{low} monocytes in CT26 tumors may explain, at least in part, why CT26 tumors are more resistant than SL4 tumors to anti-VEGF therapy and why blocking neutrophils using anti-Ly6G antibody was not sufficient to improve the antitumor efficacy of DC101 treatment (Fig. 4). Importantly, as AMD3100 targets both Ly6C^{low} monocytes and neutrophils, these findings suggest a possible route for clinical translation for improving antiangiogenic treatment of colorectal cancer therapy.

There have been several reports showing that TAMs mediate resistance to anti-VEGF therapy in different types of cancers (2, 32). It is also known that VEGF inhibition promotes maturation and activation of DCs, which leads to an increase in intratumoral effector T-cell numbers (5). In this study, we found Ly6C^{low} monocytes are the key players that drive resistance to anti-VEGFR2 therapy in colorectal cancer.

We have previously found reduced blood vessels after anti-VEGFR2 therapy (9), which indicates that alternative angiogenesis mechanisms are not the chief cause of CRC resistance to anti-VEGFR2 therapy. We have also found progressively increased hypoxia in parallel with the decrease in the intratumoral vessel density in these CRCs over the course of DC101 treatment

compared with the control (9). It has been shown that antiangiogenic treatment up-regulates the expression of CXCL12 in tumors via hypoxia (1). Indeed, the protein level of CXCL12 increased on days 5 and 12 in proportion to the degree of hypoxia (Fig. S1C). CXCL12 is also produced by tumor-infiltrating Ly6C^{low} monocytes and Ly6G⁺ neutrophils (9). We also found a predominant expression of CXCR4 in CD11b⁺ monocytes and neutrophils compared with the lymphoid populations—as measured by flow cytometry (Fig. S7). Thus, DC101 treatment appears to trigger a positive feedback loop between the expression of CXCL12 and the infiltration of CXCR4-expressing Ly6C^{low} monocytes and Ly6G⁺ neutrophils in CRCs.

Here, we showed that the blockade of CXCR4 significantly improves antitumor efficacy when combined with antiangiogenic therapy. Blockade of CXCR4 with AMD3100 treatment significantly inhibited DC101-induced tumor infiltration of Ly6C^{low} monocytes and neutrophils in both SL4 and CT26 tumors. However, AMD3100 treatment did not completely abolish infiltration of Ly6C^{low} monocytes and neutrophils. This could possibly be due to the fact that some Ly6C^{low} monocytes and neutrophils are recruited to tumors in a CXCR4-independent manner or that the dose we used to block CXCR4 signaling is not sufficiently high. Nevertheless, the majority of Ly6C^{low} monocytes and neutrophils infiltrate into the tumor in a CXCR4-dependent manner, and their infiltration can be efficiently blocked by targeting the CXCR4 axis. It would be of interest to further characterize the CXCR4-independent Ly6C^{low} monocytes and neutrophils and/or to examine the effect of a higher dose of AMD3100 on the infiltration of these cells in future studies.

Recently, we found that Ly6C^{low} monocytes and neutrophils infiltrate into tumors and confer resistance to anti-VEGFR2 therapy by secreting high amounts of immunosuppressive cytokines such as IL-10. These immunosuppressive cytokines inhibit adaptive immunity in the tumors, characterized by low numbers of CD4⁺ and CD8⁺ T cells as well as their dysfunctional phenotype (i.e., increased PD-1⁺ and reduced Granzyme B expression) (9). Consistent with this, we observed the restoration of CD4⁺ and CD8⁺ T cells and tumor growth delay when we added AMD3100

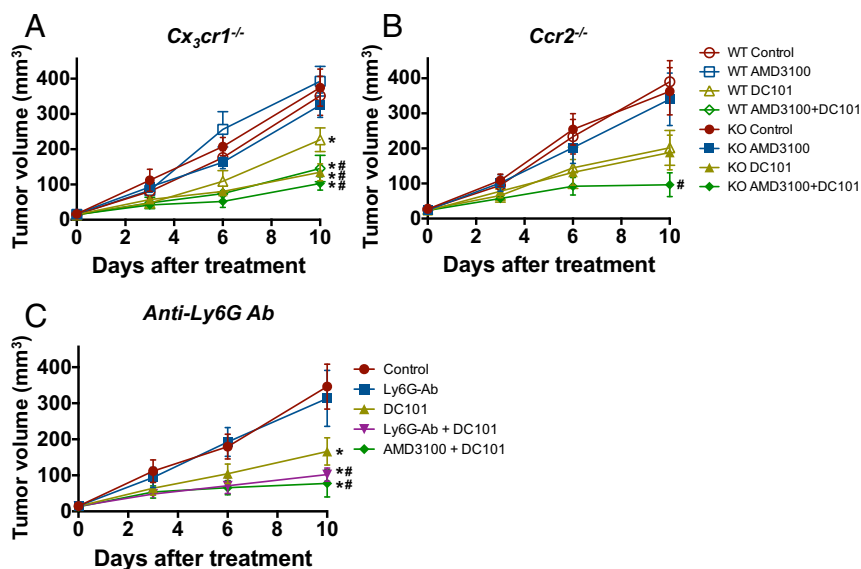


Fig. 3. CX3CR1 deletion, anti-Ly6G antibody treatment, or CXCR4 inhibition improves efficacy of anti-VEGFR2 therapy in orthotopic SL4 CRCs. (A) C57BL/6 WT or *Cx3cr1*^{-/-} (CX3CR1 KO) mice bearing SL4 CRCs were treated as indicated. Tumor volume was measured by ultrasound imaging in A–C. Data are represented as mean \pm SEM, $n = 5$ –8 per group. * $P < 0.05$ vs. WT control. # $P < 0.05$ vs. WT DC101. (B) C57BL/6 WT or *Ccr2*^{-/-} (CCR2 KO) mice bearing SL4 tumors were treated as indicated. Data are represented as mean \pm SEM, $n = 5$ –8 per group. # $P < 0.05$ vs. WT DC101. (C) The effect of administration of anti-Ly6G antibody on SL4 tumor growth. SL4 tumor-bearing C57BL/6 WT mice were treated as indicated. Data are represented as mean \pm SEM, $n = 8$ per group. * $P < 0.05$ vs. control. # $P < 0.05$ vs. DC101.

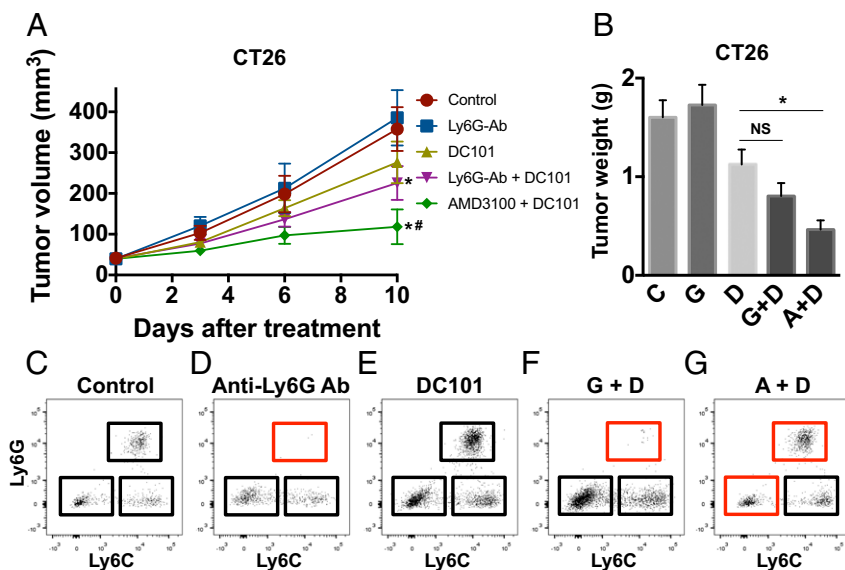


Fig. 4. CXCR4 inhibition but not anti-Ly6G antibody treatment improves efficacy of anti-VEGFR2 therapy in orthotopic CT26 CRCs. (A) The effect of administration of anti-Ly6G antibody on CT26 tumor growth. CT26 tumor-bearing BALB/c WT mice were treated as indicated. Data are represented as mean \pm SEM, $n = 8$ per group. * $P < 0.05$ vs. control. # $P < 0.05$ vs. corresponding DC101 group. (B) Tumor weight of CT26 measured on day 12 after treatment (A+D, AMD3100 + DC101; C, control; D, DC101; G, anti-Ly6G antibody; G+D, anti-Ly6G antibody + DC101). Data are represented as mean \pm SEM, $n = 8$ per group. * $P < 0.05$. NS, nonsignificant. (C–G) Representative flow cytometry plots depicting each subset of myeloid cells in CT26 tumors in (C) wild-type control mice, (D) anti-Ly6G antibody-treated mice, (E) DC101-treated mice, (F) anti-Ly6G antibody + DC101-treated mice (G+D), and (G) AMD3100 + DC101-treated mice (A+D). The red rectangles indicate depleted populations by the treatment of anti-Ly6G antibody or AMD3100.

treatment to DC101 treatment. It should be noted that the expression levels of CXCR4 on CD4⁺ and CD8⁺ T cells are very low, while CXCR4 is highly expressed in the Ly6C^{low} monocytes and Ly6G⁺ neutrophils (Fig. S7). While the blockade of CXCR4 signaling lowers the infiltration of these immunosuppressive myeloid cells and restores adaptive immune cells, the depletion of these Ly6C^{low} monocytes and neutrophils in the absence of CXCR4 blockade can also restore the number of adaptive immune cells completely (9). These findings suggest that, while the restoration of CD4⁺ and CD8⁺ T cells and their function after AMD3100 treatment results in tumor growth delay (Figs. 3 and 4), the effect on adaptive immune cells seems to be indirectly through monocytes and neutrophils via immunosuppressive cytokines such as IL-10.

The immune system plays an important role in any cancer treatment directly or indirectly (33–39). Recently, cancer immunotherapy using immune checkpoint blockers (ICBs) has revolutionized cancer therapy by curing some patients (40–42). However, the majority of cancer patients do not respond to ICBs, even in the most promising indications (41, 43). In the case of CRCs, the success of ICBs is limited to a small portion of patients with high microsatellite instability or mismatch repair-deficient cancers (44, 45). Therefore, there is an urgent need to identify intrinsic and/or acquired immunosuppression mechanisms causing resistance to ICBs and to develop novel immunotherapeutic strategies targeting such resistance mechanisms. There is mounting evidence showing that innate immune cells are actively involved in the development and progression of many types of cancers, albeit with different functions in each cancer (4, 5, 46–50). These innate immune cells are also known to play a critical role in resistance to anti-VEGF therapy in some types of cancers (2, 4). As we have shown here, the role of protumorigenic Ly6C^{low} monocytes and neutrophils in CRCs and various other types of cancers in the setting of antiangiogenic therapy in combination with ICBs should be explored further.

Collectively, we established a critical causal role of CXCR4 signaling in conferring resistance to anti-VEGFR2 therapy by recruiting Ly6C^{low} monocytes and Ly6G⁺ neutrophils to tumors and thereby skewing CRCs toward an immunosuppressive phenotype (e.g., IL-10 expression and dysfunctional cytotoxic T lymphocytes). Furthermore, we successfully inhibited recruitment of these innate immune cells by targeting the responsible pathways pharmacologically with the FDA-approved CXCR4 blocker

AMD3100, which significantly extended treatment response in clinically relevant animal models of colon cancer.

Experimental Procedures

Spontaneous Rectal Tumor Model and CRC Cell Preparation for Orthotopic CRC Models. Before implantation, we cultured SL4 (51) murine CRC cells in DMEM/F12 medium containing 10% FBS. We cultured CT26 (52) murine CRC cells in RPMI-1640 medium containing 10% FBS. We harvested subconfluent CRC cells (i.e., SL4 or CT26), and then washed the harvested cells with PBS, followed by counting the number of cells. We mixed the tumor cell suspension with the same volume of Matrigel (product no. 354262, Corning). For orthotopic SL4 CRC model, we intraperitoneally injected 100 mg/kg of ketamine and 10 mg/kg of xylazine to anesthetize 8- to 10-wk-old C57BL/6 mice. For orthotopic CT26 CRC model, we intraperitoneally injected 100 mg/kg of ketamine and 10 mg/kg of xylazine to anesthetize 8- to 10-wk-old BALB/c mice. We then removed abdominal hair using a hair clipper and made a 10-mm-long midline incision. Through the incision we exteriorized the cecum, and then injected 10 μ L of cell/Matrigel mixture containing 5×10^5 cells from the serosal side into the cecum wall between the mucosa and serosa. We used a 27-gauge needle with an insulin syringe for the cell/Matrigel mixture injection (51, 52). We put back the cecum to the abdominal cavity, closed the abdominal wall with 5-0 polysorb sutures (Covidien), and closed the skin using surgical staples. We monitored tumor size by assessing blood Gaussia luciferase (Gluc) activity (53, 54) or by using a high-frequency ultrasound imaging system two times a week. We used *Apc* conditional knockout mice as we previously described (18) for spontaneous rectal tumor model. All animal procedures followed NIH Public Health Service Policy on Humane Care and Use of Laboratory Animals and were approved by the Massachusetts General Hospital Institutional Animal Care and Use Committee.

Blood Gluc Assay for Monitoring SL4 Tumor Growth. We transduced SL4 cells with lentivirus encoding the Gluc gene to generate the SL4-Gluc cell line. We measured the activity of secreted Gluc to monitor SL4 tumor growth as described previously (53, 54). We collected blood from the tumor-bearing mice every 2 or 3 d. We used a GloMax 96 Microplate Luminometer (Promega) to measure the blood Gluc activity.

Ultrasound Imaging. We monitored tumor growth by using a high-frequency ultrasound imaging system two times a week (Vevo 2100 system, VisualSonics) using a probe with a 40-MHz frequency (MS550S) (3). We intraperitoneally injected 100 mg/kg of ketamine and 10 mg/kg of xylazine to anesthetize mice and kept them on a heated platform. We then removed abdominal hair using a hair clipper and applied ultrasound gel on the skin. We identified tumor in the cecum as a low echogenic mass and acquired images using the MS550S probe. We measured the long diameter (LD) and short diameter (SD) from the images and calculated tumor volume as $(LD \times SD^2)/2$.

Flow Cytometry. We performed flow cytometry as described previously (55). We harvested tumor tissues and chopped using a surgical scissor. We incubated chopped tissue with digestion medium containing 1.5 mg/mL of collagenase type 1A, 1.5 mg/mL of hyaluronidase, and 2 mg/mL of DNase for 1 h in a 37 °C incubator. We filtered the digested tissue using 70- μ m cell strainers followed by filtering with 40- μ m cell strainers. We incubated single cell suspensions for blocking with an anti-mouse CD16/CD32 antibody. We then stained the cell suspensions with the following antibodies: CD45 (clone 30-F11), B220 (clone RA3-6B2), CD49b (clone DX5), CD90 (clone 53–2.1), NK1.1 (clone PK136), Ter119 (clone TER-119), I-A/I-E (clone M5/114.15.2), CD4 (clone RM4-5), CD8 (clone 53–6.7), CD25 (clone PC61), FoxP3 (clone FJK-16s), CD11b (clone M1/70), F4/80 (clone BM8), CD11c (clone HL3), Gr1 (clone RB6-8C5), Ly6C (clone HK1.4), and Ly6G (clone 1A8) (BD Biosciences). We added 7-amino-actinomycin D (7AAD) reagent (eBioscience) to the stained tubes to rule out dead cells just before

running flow cytometry. Monocytes were defined as CD45⁺ Lin[−] F4/80[−] CD11c[−] CD11b⁺ Ly6C^{low} or Ly6C^{high} population. Neutrophils were defined as CD45⁺ Lin[−] F4/80[−] CD11c[−] CD11b⁺ Ly6G⁺ population. We used an LSRII flow cytometer (Becton Dickinson) and analyzed the data with FlowJo software (Tree Star).

ACKNOWLEDGMENTS. We thank Peigen Huang, John D. Martin, Sylvie Roberge, Tsion Hbatmu, and Dongjun Lee for experimental assistance and Dan Duda for helpful input. This work was supported by National Cancer Institute (NCI) Program Project Grant P01-CA080124 (to R.K.J. and D.F.) and also in part by NCI Grants R35-CA197743 (to R.K.J.), R01-CA096915 (to D.F.), NCI/Federal Share Proton Beam Program Income (to R.K.J.), NIH DP2 OD008780 (to T.P.P.), NIH R01 CA214913 (to T.P.P.), Department of Defense W81XWH-10-1-0016 (to R.K.J.), and a Tosteson Fund for Medical Discovery postdoctoral fellowship (to K.J.).

- Jain RK (2014) Antiangiogenesis strategies revisited: From starving tumors to alleviating hypoxia. *Cancer Cell* 26:605–622.
- Rivera LB, et al. (2015) Intratumoral myeloid cells regulate responsiveness and resistance to antiangiogenic therapy. *Cell Rep* 11:577–591.
- Rahbari NN, et al. (2016) Anti-VEGF therapy induces ECM remodeling and mechanical barriers to therapy in colorectal cancer liver metastases. *Sci Transl Med* 8:360ra135.
- Chung AS, et al. (2013) An interleukin-17-mediated paracrine network promotes tumor resistance to anti-angiogenic therapy. *Nat Med* 19:1114–1123.
- Rivera LB, Bergers G (2015) Intertwined regulation of angiogenesis and immunity by myeloid cells. *Trends Immunol* 36:240–249.
- Casanovas O, Hicklin DJ, Bergers G, Hanahan D (2005) Drug resistance by evasion of antiangiogenic targeting of VEGF signaling in late-stage pancreatic islet tumors. *Cancer Cell* 8:299–309.
- Sitohy B, Nagy JA, Dvorak HF (2012) Anti-VEGF/VEGFR therapy for cancer: Reassessing the target. *Cancer Res* 72:1909–1914.
- Dvorak HF (2015) Tumor stroma, tumor blood vessels, and antiangiogenesis therapy. *Cancer J* 21:237–243.
- Jung K, et al. (2017) Ly6Clo monocytes drive immunosuppression and confer resistance to anti-VEGFR2 cancer therapy. *J Clin Invest* 127:3039–3051.
- Willett CG, et al. (2009) Efficacy, safety, and biomarkers of neoadjuvant bevacizumab, radiation therapy, and fluorouracil in rectal cancer: A multidisciplinary phase II study. *J Clin Oncol* 27:3020–3026.
- Xu L, et al. (2009) Direct evidence that bevacizumab, an anti-VEGF antibody, upregulates SDF1alpha, CXCR4, CXCL6, and neuropilin 1 in tumors from patients with rectal cancer. *Cancer Res* 69:7905–7910.
- Balabanian K, et al. (2012) Proper desensitization of CXCR4 is required for lymphocyte development and peripheral compartmentalization in mice. *Blood* 119:5722–5730.
- Devi S, et al. (2013) Neutrophil mobilization via plerixafor-mediated CXCR4 inhibition arises from lung demargination and blockade of neutrophil homing to the bone marrow. *J Exp Med* 210:2321–2336.
- Eash KJ, Means JM, White DW, Link DC (2009) CXCR4 is a key regulator of neutrophil release from the bone marrow under basal and stress granulopoiesis conditions. *Blood* 113:4711–4719.
- Liu Q, et al. (2015) CXCR4 antagonist AMD3100 redistributes leukocytes from primary immune organs to secondary immune organs, lung, and blood in mice. *Eur J Immunol* 45:1855–1867.
- Martin C, et al. (2003) Chemokines acting via CXCR2 and CXCR4 control the release of neutrophils from the bone marrow and their return following senescence. *Immunity* 19:583–593.
- Chong SZ, et al. (2016) CXCR4 identifies transitional bone marrow premonocytes that replenish the mature monocyte pool for peripheral responses. *J Exp Med* 213:2293–2314.
- Kim P, et al. (2010) In vivo wide-area cellular imaging by side-view endomicroscopy. *Nat Methods* 7:303–305.
- Donzella GA, et al. (1998) AMD3100, a small molecule inhibitor of HIV-1 entry via the CXCR4 co-receptor. *Nat Med* 4:72–77.
- Duda DG, et al. (2011) CXCL12 (SDF1alpha)-CXCR4/CXCR7 pathway inhibition: An emerging sensitizer for anticancer therapies? *Clin Cancer Res* 17:2074–2080.
- Yang L, et al. (2008) Abrogation of TGF beta signaling in mammary carcinomas recruits Gr-1+CD11b+ myeloid cells that promote metastasis. *Cancer Cell* 13:23–35.
- Kumar A, et al. (2006) CXCR4 physically associates with the T cell receptor to signal in T cells. *Immunity* 25:213–224.
- Thelen M (2001) Dancing to the tune of chemokines. *Nat Immunol* 2:129–134.
- Hiratsuka S, et al. (2011) C-X-C receptor type 4 promotes metastasis by activating p38 mitogen-activated protein kinase in myeloid differentiation antigen (Gr-1)-positive cells. *Proc Natl Acad Sci USA* 108:302–307.
- Shojaei F, et al. (2007) Tumor refractoriness to anti-VEGF treatment is mediated by CD11b+Gr1+ myeloid cells. *Nat Biotechnol* 25:911–920.
- Nahrendorf M, et al. (2007) The healing myocardium sequentially mobilizes two monocyte subsets with divergent and complementary functions. *J Exp Med* 204:3037–3047.
- Geissmann F, Jung S, Littman DR (2003) Blood monocytes consist of two principal subsets with distinct migratory properties. *Immunity* 19:71–82.
- Carlin LM, et al. (2013) Nr4a1-dependent Ly6C(low) monocytes monitor endothelial cells and orchestrate their disposal. *Cell* 153:362–375.
- Jung S, et al. (2000) Analysis of fractalkine receptor CX(3)CR1 function by targeted deletion and green fluorescent protein reporter gene insertion. *Mol Cell Biol* 20:4106–4114.
- Jung K, et al. (2013) Endoscopic time-lapse imaging of immune cells in infarcted mouse hearts. *Circ Res* 112:891–899.
- Willett CG, et al. (2004) Direct evidence that the VEGF-specific antibody bevacizumab has antivasculature effects in human rectal cancer. *Nat Med* 10:145–147.
- Rigamonti N, et al. (2014) Role of angiopoietin-2 in adaptive tumor resistance to VEGF signaling blockade. *Cell Rep* 8:696–706.
- Pardoll D (2015) Cancer and the immune system: Basic concepts and targets for intervention. *Semin Oncol* 42:523–538.
- Kumar V, Patel S, Tcyganov E, Gabrilovich DI (2016) The nature of myeloid-derived suppressor cells in the tumor microenvironment. *Trends Immunol* 37:208–220.
- Hanahan D, Coussens LM (2012) Accessories to the crime: Functions of cells recruited to the tumor microenvironment. *Cancer Cell* 21:309–322.
- Noy R, Pollard JW (2014) Tumor-associated macrophages: From mechanisms to therapy. *Immunity* 41:49–61.
- Palucka AK, Coussens LM (2016) The basis of oncoimmunology. *Cell* 164:1233–1247.
- Ghosh M, et al. (2009) PPARdelta is pro-tumorigenic in a mouse model of COX-2-induced mammary cancer. *Prostaglandins Other Lipid Mediat* 88:97–100.
- Proia RL, Hla T (2015) Emerging biology of sphingosine-1-phosphate: Its role in pathogenesis and therapy. *J Clin Invest* 125:1379–1387.
- Buchbinder EI, Hodi FS (2016) Melanoma in 2015: Immune-checkpoint blockade - durable cancer control. *Nat Rev Clin Oncol* 13:77–78.
- Baumeister SH, Freeman GJ, Dranoff G, Sharpe AH (2016) Coinhibitory pathways in immunotherapy for cancer. *Annu Rev Immunol* 34:539–573.
- Topalian SL, Taube JM, Anders RA, Pardoll DM (2016) Mechanism-driven biomarkers to guide immune checkpoint blockade in cancer therapy. *Nat Rev Cancer* 16:275–287.
- Pardoll DM (2012) The blockade of immune checkpoints in cancer immunotherapy. *Nat Rev Cancer* 12:252–264.
- Liosa NJ, et al. (2015) The vigorous immune microenvironment of microsatellite instable colon cancer is balanced by multiple counter-inhibitory checkpoints. *Cancer Discov* 5:43–51.
- Xiao Y, Freeman GJ (2015) The microsatellite instable subset of colorectal cancer is a particularly good candidate for checkpoint blockade immunotherapy. *Cancer Discov* 5:16–18.
- Talmadge JE, Gabrilovich DI (2013) History of myeloid-derived suppressor cells. *Nat Rev Cancer* 13:739–752.
- Schmid MC, Varner JA (2012) Myeloid cells in tumor inflammation. *Vasc Cell* 4:14.
- Engblom C, Pfirschke C, Pittet MJ (2016) The role of myeloid cells in cancer therapies. *Nat Rev Cancer* 16:447–462.
- Kaneda MM, et al. (2016) PI3K γ is a molecular switch that controls immune suppression. *Nature* 539:437–442.
- Kaneda MM, et al. (2016) Macrophage PI3K γ drives pancreatic ductal adenocarcinoma progression. *Cancer Discov* 6:870–885.
- Morimoto-Tomita M, Ohashi Y, Matsubara A, Tsuiji M, Irimura T (2005) Mouse colon carcinoma cells established for high incidence of experimental hepatic metastasis exhibit accelerated and anchorage-independent growth. *Clin Exp Metastasis* 22:513–521.
- Zhang Y, Davis C, Ryan J, Janney C, Peña MM (2013) Development and characterization of a reliable mouse model of colorectal cancer metastasis to the liver. *Clin Exp Metastasis* 30:903–918.
- Chung E, et al. (2009) Secreted Gaussia luciferase as a biomarker for monitoring tumor progression and treatment response of systemic metastases. *PLoS One* 4:e8316.
- Tannous BA (2009) Gaussia luciferase reporter assay for monitoring biological processes in culture and in vivo. *Nat Protoc* 4:582–591.
- Huang Y, et al. (2012) Vascular normalizing doses of antiangiogenic treatment reprogram the immunosuppressive tumor microenvironment and enhance immunotherapy. *Proc Natl Acad Sci USA* 109:17561–17566.